Effects of environmental factors on the monitoring of environmental radioactivity by airborne gamma-ray spectrometry

Julien Amestoy, Pierre-Yves Meslin, Patrick Richon, Aude Delpuech, Solène Derrien, Hugo Raynal, Éric Pique, David Baratoux, Pascal Chotard, Pieter van Beek, et al.

Journal of Environmental Radioactivity 237 (2021) 106695

Contents lists available at ScienceDirect

Journal of Environmental Radioactivity

journal homepage: www.elsevier.com/locate/jenvrad

Effects of environmental factors on the monitoring of environmental radioactivity by airborne gamma-ray spectrometry

Julien Amestoy [a,b,*], Pierre-Yves Meslin [a], Patrick Richon [b], Aude Delpuech [b], Solène Derrien [c], Hugo Raynal [a,c], Éric Pique [c], David Baratoux [d], Pascal Chotard [b], Pieter Van Beek [e], Marc Souhaut [e], Thomas Zambardi [e]

[a] Institut de Recherche en Astrophysique et Planétologie, Université de Toulouse, CNRS, UPS, CNES, Observatoire Midi-Pyrénées, Toulouse, France
[b] CEA, DAM, DIF, F-91297, Arpajon – Cedex, France
[c] Laboratoire d'Aérologie, Université de Toulouse, CNRS, Observatoire Midi-Pyrénées, Toulouse, France
[d] Géosciences Environnement Toulouse, Université de Toulouse, Observatoire Midi-Pyrénées, CNRS, IRD, Toulouse, France
[e] Laboratoire d'Études en Géophysique et en Océanographie Spatiale, Université de Toulouse, CNES, CNRS, IRD, UPS, Observatoire Midi-Pyrénées, Toulouse, France

ARTICLE INFO

Keywords:
Airborne gamma-ray spectrometry
Environmental factors
NaI(Tl) detector
Atmospheric radon-222
Soil moisture
Uranium
Thorium
Potassium
Cosmic rays

ABSTRACT

This study describes and discusses the results of a 14 month-long campaign (April 2019 to June 2020) aimed at characterizing and quantifying the influence of environmental factors (cosmic rays, rainfall events, soil moisture and atmospheric radon) on airborne radiometric surveys, which are used for mapping the concentrations of potassium (K), uranium (U) and thorium (Th), or for monitoring the natural radioactivity in the environment. A large NaI(Tl) airborne spectrometer (4 down + 1 up detectors of 4 L) was installed at a height of 50 m on a meteorological tower to simulate an airborne hover at the Pyrenean Platform for Observation of the Atmosphere (P2OA) in Lannemezan. The continuous, high frequency acquisition of gamma-rays was accompanied by measurements of rainfall intensity, soil moisture content, atmospheric radon activity and meteorological parameters. A semi-diurnal cycle of apparent ^{232}Th and ^{40}K was observed and explained by atmospheric thermal tides. Both diurnal and seasonal cycles are also evident in the gamma-ray signal, mostly due to variations of soil moisture at these timescales with a maximum during summer when surface soil moisture (0–5 cm depth) is the lowest. An increase of 25% vol. of the soil moisture content, representing the range of variation between the end of summer (18% vol.) and the beginning of spring (43% vol.) leads to a decrease of gamma-rays in the K and Th window by the same amount. Conversely, these results illustrate the potential of using airborne gamma-ray spectrometry to monitor soil moisture at hectometer scales. The washout of radon-222 progeny during rainfall events influences the count of gamma-rays in the U window by adding an atmospheric component to the soil component. The amplitude of the signal increase in the U window varies with the precipitation rate and reaches 30% for an average event. By clear weather, atmospheric radon-222 volumic activity influences the count rate in the U window by about ±3.8% per Bq m^{-3}, which translates into an influence of 148%/Bq m^{-3}/kg Bq^{-1} (U). This comprehensive, multi-compartment approach is necessary to optimize and improve the processing and analysis of airborne gamma-ray spectrometry data for high sensitivity environmental studies. These results show the importance of environmental factors on the variability of gamma-ray spectrometry and the importance of taking them into account to accurately map radionuclides activities.

1. Introduction

The presence of gamma-emitting radionuclides in soils and the large penetration depth of gamma radiation in air have long been considered for the detection and quantification of natural and artificial radionuclides by airborne gamma-ray spectrometry. Outside incidental or accidental situations, the main radionuclides present in the ground are ^{40}K, ^{238}U (+progeny), ^{232}Th (+progeny) and ^{137}Cs.

Typical applications of airborne gamma-ray spectrometry include radioactive mineral exploration (Grasty, 1975; Tourlière et al., 2003),

* Corresponding author. Institut de Recherche en Astrophysique et Planétologie, Université de Toulouse, CNRS, UPS, CNES, Observatoire Midi-Pyrénées, Toulouse, France.
E-mail address: julien.amestoy@cea.fr (J. Amestoy).

https://doi.org/10.1016/j.jenvrad.2021.106695
Received 3 December 2020; Received in revised form 17 June 2021; Accepted 26 June 2021
Available online 28 July 2021

radiological survey following nuclear incidents or accidents (Grasty et al., 1997; Sanada and Torii, 2015), geological mapping, study of weathering processes (Carrier et al., 2006; Wilford, 2012), soil mapping (Cook et al., 1996; Wilford et al., 1997), search for radioactive sources (Deal et al., 1972) and study of the anthropogenic influence on its environment, like agricultural fertilization practices (Punniyakotti et al., 2020).

In order to monitor the concentrations of thorium (Th), uranium (U) and potassium (K) in the ground, the International Atomic Energy Agency recommended a three window method presented in Table 1 (IAEA, 1991). Thorium and U are measured indirectly with gamma-ray-emitting decay products in their respective decay series. Thorium is measured from gamma radiation emitted by ^{208}Tl at 2615 keV, U from ^{214}Bi at 1764 keV and K is detected directly from 1461 keV gamma-rays emitted by ^{40}K. Since gamma-ray spectrometry is sensitive to environmental conditions, which can vary from one campaign to another, the concentration maps obtained by this geophysical technique are, strictly speaking, and without further correction, only valid for a specific day, and even for a specific time of the day.

The variation of the count rates with soil moisture for a soil with uniform radionuclides distribution has been documented by laboratory studies and by individual airborne surveys (Kogan et al., 1971; Carroll, 1981; Beamish, 2015). These studies, which were carried out over the typical time scale of an airborne survey, confirmed the expected decrease of the gamma-ray flux from K, Th (and U) with increasing soil moisture. The presence of free or adsorbed water in the soil pore space increases its bulk density and thus its attenuation coefficient (e.g. Løvborg, 1984; Grasty, 1997). As a result, uncertainties or variations of soil moisture can represent a significant source of error in interpreting gamma-ray surveys in terms of K, Th and U concentration in the (dry) soil. An increase in volumetric soil moisture (relative volume of water in a unit volume of soil) of 10% decreases the measured fluence rate by about the same amount (Minty, 1997). A proximal gamma-ray spectroscopy study also investigated the possibility to use this technique for assessing soil water content (Baldoncini et al., 2019). It was applied to study the effect of the biomass water content on soil moisture in a bare soil through a 7 month continuous campaign.

Another environmental parameter affecting airborne gamma-ray spectrometry is related to the transport of radon-222 (hereafter referred to as radon), a naturally occurring noble gas from the U decay series, and the radioactive α-decay product of long-lived ^{226}Ra mostly present in rocks and soils. Radon-222 emanated from the ground can diffuse through the soil porosity and reach the atmosphere, producing short live daughters, such as ^{214}Bi, which are subject to aerosol attachment, possible detachment by recoil, and deposition. These mechanisms will influence the measurement of ^{214}Bi by adding an atmospheric component to the ground component. Radon-222 concentration in the atmosphere varies daily and seasonally due to changes in the exhalation rate associated with fluctuations of soil humidity and due to variations of meteorological parameters at local and regional scales. In the analysis of airborne data, this time-variable atmospheric component contributes to the intensity of the ^{214}Bi signal and needs to be substracted from the raw data. Although the influence of atmospheric radon-222 on the U window has long been recognized, it has rarely been studied in details and, to our knowledge, is not routinely and even very seldom corrected for.

Table 1
Spectral windows used to measure K, U and Th recommended by the IAEA, 1991.

Element	Isotope	Gamma-ray energy (keV)	Energy window (keV)
Potassium	^{40}K	1461	1370–1570
Uranium	^{214}Bi	1764	1660–1860
Thorium	^{208}Tl	2615	2410–2810
Total Count	–	–	40–2810

Some of the airborne gamma-ray spectrometry applications require multi-annual monitoring, which in turn requires a detailed understanding of all environmental and instrumental parameters that can induce temporal variations for subsequent corrections. In order to better understand these parameters, we are conducting a multi-annual, multi-compartment survey of the environmental radioactivity at the Pyrenean Platform for Observation of the Atmosphere on the Centre de Recherches Atmosphériques (P2OA-CRA) site, in Lannemezan, France.

The purpose of this survey is to simulate a long-lasting (>1 year) hover flight of an airborne gamma-ray system with a 20 L NaI(Tl)-type gamma-ray spectrometer installed on a 60 m tall meteorological mast. The atmospheric and soil compartments are also monitored to characterize the temporal variations of the airborne gamma-ray signal and to assess the effect of radon, rainfall and soil humidity. Although the influence of these environmental factors on the gamma-ray signal were already well-documented, the very long duration of this airborne gamma-ray spectroscopy campaign at a height of 50 m, and the independent monitoring and characterization of each compartment (soil and atmosphere) characterize the uniqueness of this work.

In this paper, we summarize the trends observed in a 14 month-long time series of continuous gamma-ray signal acquisitions at P2OA-CRA (from April 2019 to June 2020), in conjunction with associated environmental measurements.

Future studies will be focused on the implementation and validation of specific corrections to account for the effect of each environmental factor on the gamma-ray signal.

2. Materials and methods

2.1. Site description

2.1.1. Overall context

All measurements were performed at the Pyrenean Platform for Observation of the Atmosphere on the Centre de Recherches Atmosphériques (hereafter referred to as P2OA-CRA) in Lannemezan (43° 07′ 26″N, 0° 22′ 44″E), in the Southwest of France near the Pyrénées mountains (Fig. 1). The P2OA-CRA is located in the sedimentary plateau of Lannemezan, at an altitude varying between 580 and 600 m above sea level. The P2OA-CRA covers a flat area of 70 ha on permanent and temporary grasslands. The vicinity of P2OA-CRA is characterized by a low anthropogenic impact with some corn and cereal fields and coniferous forest. A temperate continental climate with local oceanic influences is dominant in this area. The mean annual temperature is about 12.4 °C, while the mean annual precipitation rate varies between 1000 and 1100 mm.

The P2OA-CRA is the instrumental site of the Laboratoire d'Aérologie of Toulouse and belongs to the Université Paul Sabatier, Toulouse, France. A 60 m-tall meteorological mast is present on the field site. The continuous monitoring network on the mast provides real time meteorological parameters such as pressure (with a frequency of 0.1 Hz), air temperature (0.1 Hz), horizontal and vertical wind speeds (at 0.1 Hz), and traces gases (H_2O, CO_2, CH_4, CO) at 1 Hz, at different heights (0 m, 2 m, 5 m, 30 m and 60 m). A bucket rain gauge with a 0.2 mm tilt-in sensitivity is also connected to the network to measure the intensity of rainfall events.

2.1.2. Radiological context

A pedestrian gamma survey of the field site was conducted around the meteorological mast over a week. The purpose was to reconstruct the soil total count rate, in c s^{-1}, over the sensitivity area of the spectrometer in order to map the spatial variations of the soil radioactivity.

The survey consisted of 1 s measurements of the total count in a 60–1500 keV window, with a fixed distance between the NaI(Tl) gamma probe (CREMP©, size of the crystal = 2.0 inch–5.08 cm - in diameter and 0.5 inch–1.27 cm - in thickness) and the ground surface of 20 cm, following grid lines that were ~1 m apart. The depth of soil investigated

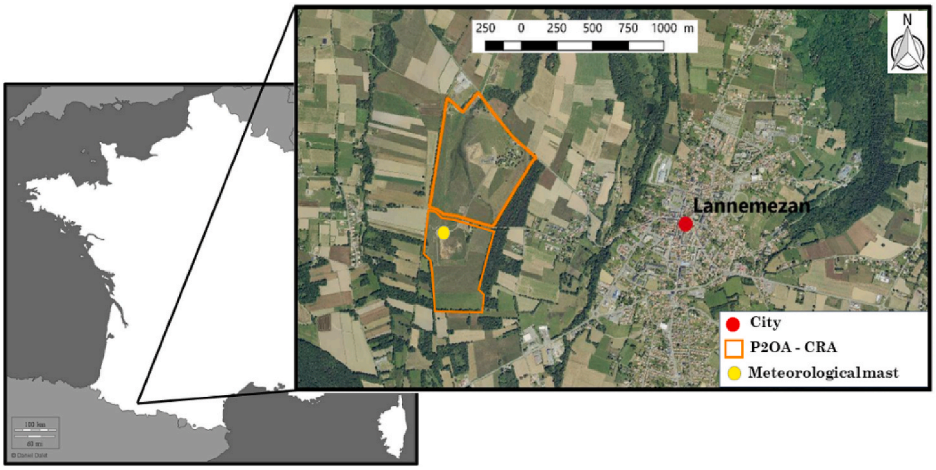

Fig. 1. Maps indicating the location of the Centre de Recherches Atmosphériques (P2OA-CRA) site and the 60 m meteorological mast. Source: Géoportail.

with this pedestrian protocol is around 20 cm. The weather conditions, cold and cloudy, were approximately similar during the survey with a relative stable volumic soil moisture of 35%.

The interpolated map of the 45000 m^2 area covered around the mast (Fig. 2) shows some spatial variations with a total count rate ranging from 60 to 160 c s^{-1}. The lowest values (60–80 c s^{-1}) coincide with permanent grassland developed on deep soil. The highest values (140–160 c s^{-1}) are representative of the soil parent material in this area, a typical clay loam (red zone in Fig. 2), which was exposed following a land levelling operation. Most of the areas characterized by a total count rate varying between 110 and 130 c s^{-1} are associated with deep parent material remobilized to the surface, like in the vicinity of the mast anchors points, on the gravel access road and around the artificial drainage stream (Fig. 2).

This interpolated radiological map guided the selection of 112 soil samples in the different "radiological units" over the full range of variations observed and from the top soil to 1-m deep. These samples were dried at 105 °C for 24 h and were analyzed in the underground Low Radioactivity laboratory LAFARA (LAboratoire de mesure des FAibles RAdioactivités) with a calibrated Germanium detector. A 24 h measurement time and the same conditioning protocol are used for each sample. The average weight is 24.2 g.

The soil around the meteorological mast consists of a uniform 1 m-deep brunisol or veracrisol with a median activity of K, Th and U, expressed as Bq kg^{-1} dry soil, of 260.5 ± 27.8, 44.3 ± 3.2 and 37.9 ± 5.7. These median values are higher than the worldwide median for ^{232}Th and ^{238}U of 30 and 35 Bg kg^{-1}, but lower than the median for ^{40}K, of 400 Bq kg^{-1} (Table 2) (UNSCEAR, 2000a). The mean activity concentrations of K, Th and U expressed as Bq kg^{-1} dry soil are 290.1 ± 29.4., 45.4 ± 3.3 and 38.9 ± 5.7. The P2OA-CRA soils are typical for a continental area.

The activity concentrations of K, U and Th are relatively constant between soils taken from different depths for the uniform 1 m-deep brunisol or veracrisol, ranging from 233 ± 24 to 261 ± 28 Bq kg^{-1}, 36 ± 5 to 41 ± 7 Bq kg^{-1} and 38 ± 0.9 to 43 ± 1.2 Bq kg^{-1} respectively. A larger activity concentration is observed for U in the topsoil near the anchor points and the artificial drainage system, due to reworking of soil

Table 2
Median values for ^{232}Th, ^{238}U and ^{40}K expressed in Bq kg^{-1} for the 112 soil samples collected at P2OA-CRA compared to the worldwide soil median (UNSCEAR, 2000a; 2000b).

	Lannemezan median Bq kg^{-1}	Worldwide median Bq kg^{-1}
^{232}Th	44.3 ± 3.2	30
^{238}U	37.9 ± 5.7	35
^{40}K	260.5 ± 27.8	400

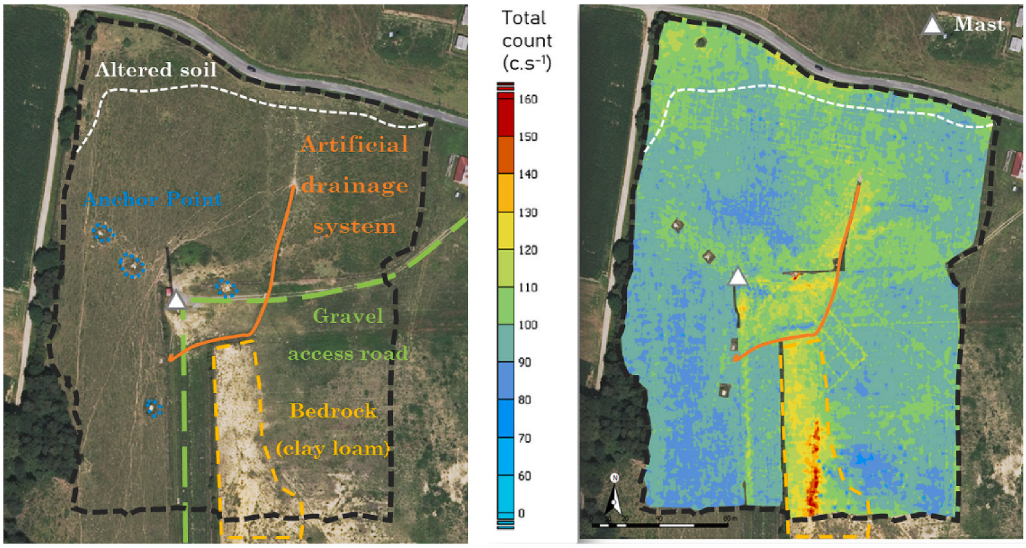

Fig. 2. Interpolated map (Kartotrak®) for the total count in c s^{-1} for the energy range 60–1500 keV with the gamma pedestrian system CREMP©. The selected site shows spatial variations around the mast ranging from 60 to 160 c s^{-1}. The highest values are located on the clay loam, which is the parental material of the surrounding soil that developed *in situ*. The scattered vegetation on the clay loam is related to the presence of a temporary wetland 6–8 month per year. Anchor points refer to concrete pads connected to the mast by tensioned cables to stabilize the tower.

in these areas, and tends to be related to the higher total count in these areas (Fig. 2). A correlation between the largest Th contents of soil samples and the largest total count rates is observed for the bedrock.

2.2. Gamma-ray measurement instrumentation

Thallium-activated sodium iodide (NaI(Tl)) scintillators have been widely used for airborne gamma-ray spectrometry. Indeed, although they have a quite poor energy resolution, they offer ruggedness for long-term outdoor operations and they can be built with relatively large volumes with high scintillation efficiency, to provide the high detection efficiency and high acquisition rate (1s) required for the detection and measurement of low-level radiation from both natural and artificial sources with a fast-moving aircraft.

In order to monitor fine-scale time variations of the signal, we used the RSX-5-20 L NaI(Tl)-type gamma-ray spectrometer from Radiations Solutions Inc., Canada. The detector is composed of 4 crystals (4 x 4 L) covered by a 5th crystal (4 L). The 4 crystals are referred to as the "Down" component of the spectrometer. The 5th crystal (or top crystal, referred to as the "Up" component) is intended to correct for the radon-222 background (Fig. 3). However, such a correction, based on our knowledge of the literature, has never been implemented.

A complete calibration procedure to determine the detection efficiency of the instrument for ^{232}Th (^{208}Tl), ^{238}U (^{214}Bi) was carried out. We performed a 4π steradians calibration where the scintillator was placed at the centre of a mechanical support and a total of 11 radioactives sources were used (^{241}Am, ^{133}Ba, ^{207}Bi, ^{60}Co, ^{137}Cs, ^{152}Eu, ^{22}Na, ^{228}Th, ^{232}Th, ^{238}U). The distance between the source and the centre of the detector was fixed at 0.98 m. For each source, 80 measurement points on a sphere were recorded for a time varying between 60 s and 300 s according to the activity of the radioactive source (Fig. 4). The intrinsic background of the 5 crystals, which corresponds to radiation produced by trace amounts of Th, U and K present in the detector and in materials forming the instrument, was measured by placing the scintillator in a lead castle built with 350 archaeological lead bricks (total thickness of 10 cm) to isolate it from the external radiation sources (Fig. 4). The intrinsic background was found to be 3.4 c s^{-1} for ^{232}Th (^{208}Tl), 2.7 c s^{-1} for ^{238}U (^{214}Bi) and 3.3 c s^{-1} for ^{40}K. The scintillation detector has a resolution of ~7% at 662 keV (^{137}Cs) and ~4% at 2615 keV (^{232}Th (^{208}Tl)), which are typical values for this type and volume of detector. The high voltage gain is automatically adjusted using natural ^{232}Th (^{208}Tl) and we controlled it by daily checks and kept records of its evolution.

The NaI(Tl) detector was installed at a height of 50 m on an aluminum mechanical support mounted on a freight elevator whose height is fixed with a winch (Fig. 4). The NaI(Tl) detector and its power supply are protected by a 2 mm aluminum cover on top of its carbon fiber housing, covering only the upper part and the sides of the instrument. An Ethernet cable connects the NaI(Tl) detector to a computer and allows continuous communication with the instrument and data reception. Continuous data acquisition was obtained over a 14 month-period, from April 30, 2019 to June 30, 2020 with an integration time of 1 s. The instrument did not exhibit any signs of wear over this whole time period. In particular, it worked perfectly during the warmest period ever recorded in France (June 2019). The air temperature varied between −4 °C and +35 °C and the sensor temperature from +18 °C to 63 °C. The instrument also underwent very large and repeated humidity variations without showing any signs of hygroscopic-induced degradation. Over this 14 month-period, only ~50 h of data (~0.5%) were lost, mostly due to short power outages.

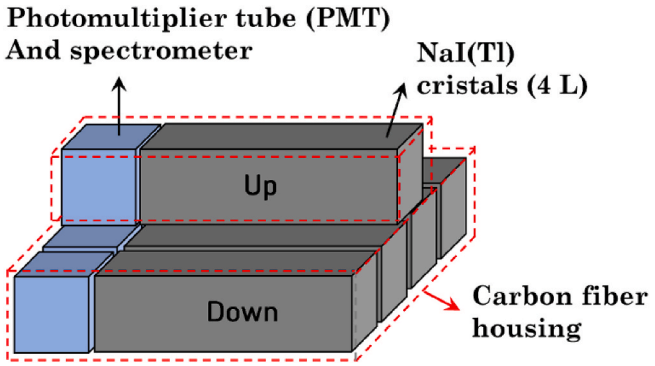

Fig. 3. NaI(Tl) RSX5 spectrometer (Radiations Solutions Inc.).

The standard procedure for airborne gamma-ray spectrometric mapping with NaI(Tl) scintillators is to use a 1 s integration time. Although spectra were recorded every second, we also integrated spectra every 30 s, since the instrument was stationary and only aimed at measuring temporal variations. For each 30 s spectrum, after subtracting the intrinsic and cosmic background, the net count rate is retrieved in the main ^{232}Th (^{208}Tl), ^{238}U (^{214}Bi) and ^{40}K photopeak energy windows (IAEA, 2003). Then, an hourly average of these count rates was computed to match the integration time of other instruments. All measurements were recorded on a UTC time reference, since the daily radon and humidity cycles, for example, are related to the true solar time, which is closer to the UTC time at Lannemezan. The choice to switch to UTC allows a reliable and durable synchronization of the instruments, in particular because time changes are avoided.

2.3. Radon measurement instrumentation

To assess the time-dependent effect of radon on the gamma signal, we equipped the mast at three heights (1 m, 30 m and 60 m) with calibrated radon detectors (Fig. 4). The same type of radon monitor (AlphaGuard PQ2000Pro, from Saphymo) was deployed at each height, in an open protective housing.

The AlphaGuard PQ2000Pro is a complete on-site system for radon measurement. It monitors radon in the ambient air using an ionization chamber of known volume (0.56 L), after filtering radon progenies. A standard diffusion mode was used rather than a flux mode.

A continuous measurement over 19 months from December 4, 2018 to June 30, 2020, with an integration time of 1 h was recorded. An hourly average value from the three AlphaGuards was then calculated. Before their installation on the mast, a complete calibration campaign including background characterization (100 h-long measurements under N_2 flow) and absolute volume activity calculation was performed for each instrument. Atmospheric pressure, air temperature and relative humidity were also recorded by these AlphaGuards. Their detection limit for an integration time of 1 h is started to be 2 Bq m^{-3} by the manufacturer (in diffusion mode), but lower detection limits can be reached by averaging the measurements from several detectors (three in our case, which should yield a detection limit of ~1.15 Bq m^{-3}) and by extending the integration time.

Each instrument is connected to a computer with a RS232 cable, which allows the communication with the instruments and the data collection.

Over the 19 months of the campaign, no data were lost, despite short power outages, due to their large storage memory.

2.4. Soil moisture instrumentation

In order to evaluate the impact of soil moisture on the gamma-ray signal, a complete soil humidity measurement system was deployed on the field.

This system consists of nine soil moisture sensors inserted at different depths in the soil and a data logger to save all the 10-min measurements (Fig. 3). Each probe employs time domain reflectometry (TDR) to measure volumetric moisture content in the soil. It is an indirect measurement based on the correlation between the signal from the probe and the dielectric properties of the material in which they are inserted.

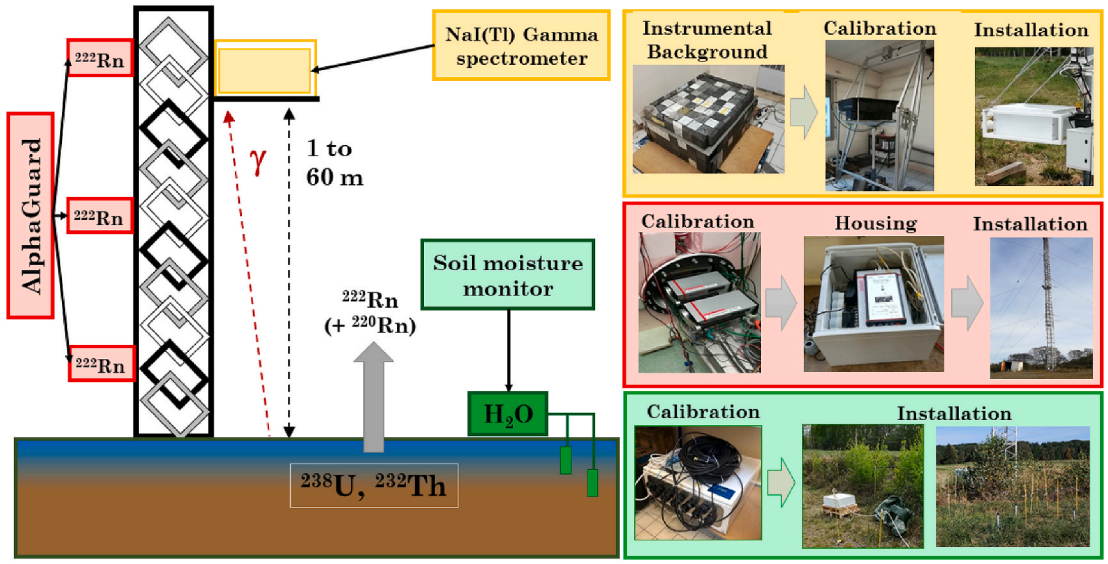

Fig. 4. Instruments installed on the 60 m-meteorological mast and around. The upper inlet depicts the background measurement calibration and deployment of the NaI(Tl) gamma spectrometer. The middle inlet illustrates the calibration and deployment of the AlphaGuards. The soil moisture monitoring system is shown in the bottom frame.

The soil moisture is deduced from the soil permittivity after calibration with the material of interest. This calibration procedure was performed in the laboratory with collected soil samples. The system was installed around the meteorological mast and the bucket rain gauge. Three probes spaced 2 m apart were deployed at a depth of 0–5 cm to monitor the surface soil moisture. Data from these probes were averaged over each 10-min period. An average value of these three values of surface soil humidities was calculated. The other sensors were used to monitor a soil moisture profile from 0 to 50 cm depth, every 10 cm in depth. The six 10-min measurements were averaged to calculate an hourly soil moisture humidity value.

Like for the gamma-ray spectrometer, a continuous acquisition over 14 months, from April 30, 2019 to June 30, 2020 was recorded for each probe. Only 15 days were not recorded during this time period, during

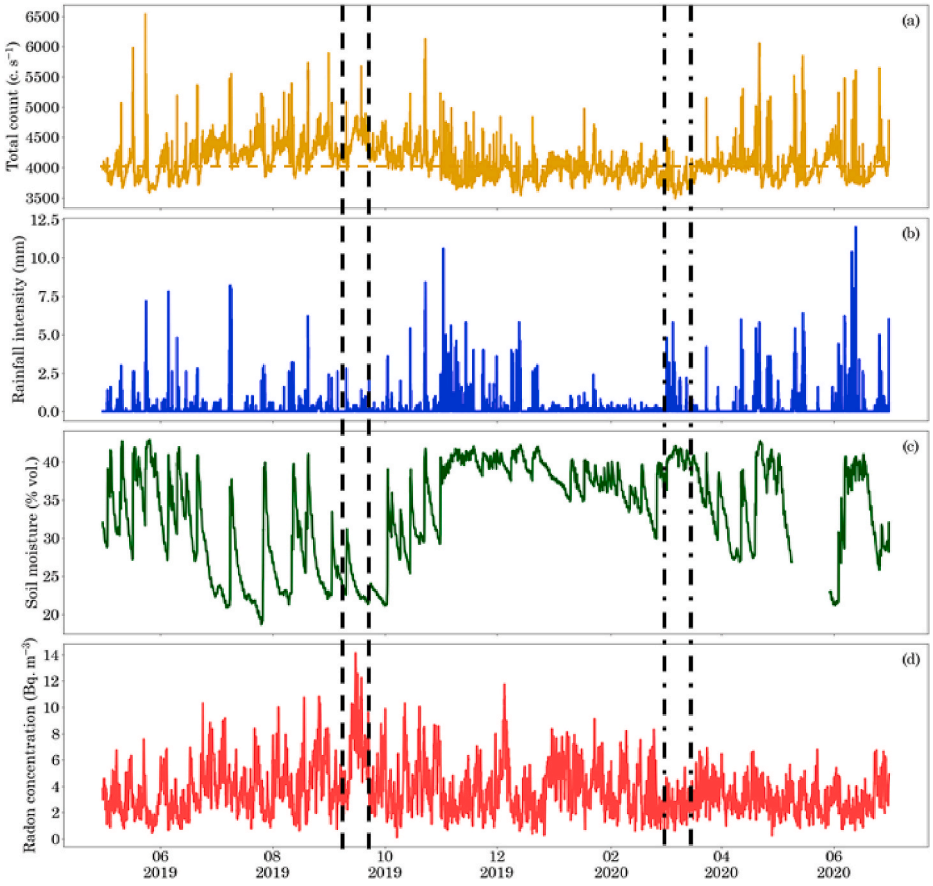

Fig. 5. Time series (1 h sampling time) of (a) Total count in c s^{-1} (the dashed lines represents the yearly average). (b) Rainfall intensity in mm h^{-1}, (c) Soil moisture content over the 0–5 cm depth range in % vol. and (d) Atmospheric radon concentration in Bq m^{-3} as recorded at the Centre de Recherches Atmosphériques (P2OA-CRA) in Lannemezan between April 2019 and June 2020. The black dashed lines represent the seasonal maximum and the black dashed dotted lines, the seasonal minimum.

the Covid-19 “Great Lockdown” in France.

2.5. Data processing

A dedicated software was developed to post-process the recorded gamma spectra: energy calibration, intrinsic and cosmic background subtraction, generation of 1 h-long spectra and calculation of the net count rates in the energy windows of ^{232}Th (^{208}Tl), ^{238}U (^{214}Bi) and ^{40}K (Table 1).

3. Results and discussion

The results presented in this section refer to a set of 10152 hourly averaged gamma-ray count from the « Down » component of the spectrometer (Total count, ^{232}Th (^{208}Tl), ^{238}U (^{214}Bi), ^{40}K), atmospheric radon concentrations, soil moisture contents (vol% of H_2O of free porosity) and atmospheric pressure over a period of continuous observation from April 2019 to June 2020. The corresponding time series are shown in Fig. 5.

3.1. Temporal characterization of the gamma-ray signal, radon concentration and soil moisture records

The time series of the gamma-ray spectra total counts shows some diurnal and seasonal variations. Outside rainfall events, which are associated with spikes in the total count rate, the latter varies between 3600 and 4500 c s^{-1} (Fig. 5a), *i.e.*, shows 25% variations around its yearly average. The largest temporary increases of the total count rate (Fig. 5b) are synchronous to rainfall events and thus also to increases of the soil moisture content (Fig. 5c). Soil moisture content in the 0–5 cm depth range shows a 25% absolute difference between the minimum (18%) and the maximum (43%) observed values (Fig. 5c). Atmospheric radon-222 activities range from 0.5 Bq m^{-3} to 14 Bq m^{-3}.

The 14 month-record exhibits a clear annual cycle with a maximum of the “baseline” total counts during the end of summer-beginning of fall (black dashed lines in Fig. 5) and a minimum signal during the end of winter-beginning of spring (black dashed dotted lines in Fig. 5). The seasonal maximum of total count (4500 c s^{-1}), rainfall events excluded, coincides with the minimum values of soil moisture (20%) and the maximum of atmospheric radon (14 Bq m^{-3}). Conversely, atmospheric radon reaches lower mean values when soil moisture is higher in winter and spring, in spite of the shallower thickness of the atmospheric boundary layer that tends to increase the near-surface radon concentration during winter, and the total count signal reaches its lowest value of the year.

The monthly averages of all the measured quantities (Fig. 6) confirm the seasonal pattern observed in Fig. 5. Rainfall events, identified whenever a non-zero value is recorded by the rain gauge, are excluded from these monthly means not to take into account the effect of the washout of radon-222 progeny on the monthly total count rates (See section 2.1.2).

The total count rate and the count rates for ^{232}Th, ^{238}U, ^{40}K, reach a maximum at the beginning of fall, particularly in October (4350, 32, 20.4, 53.9 c s^{-1}, respectively), while the soil moisture content reaches its minimum (24%). Between November and December 2019, a strong decrease of all the gamma signals is observed: −11.25% for the total count rate (relative to its average), −12.28% for ^{232}Th counts, −7.03% for ^{238}U counts and −13.26% for ^{40}K, while the soil moisture increases by 16%. The observed decrease for uranium counts is limited in comparison to potassium and thorium counts. The presence of a relatively high concentration of atmospheric radon-222 (3–4.5 Bq m^{-3}), especially in February 2020, could influence the measurement of ^{214}Bi by

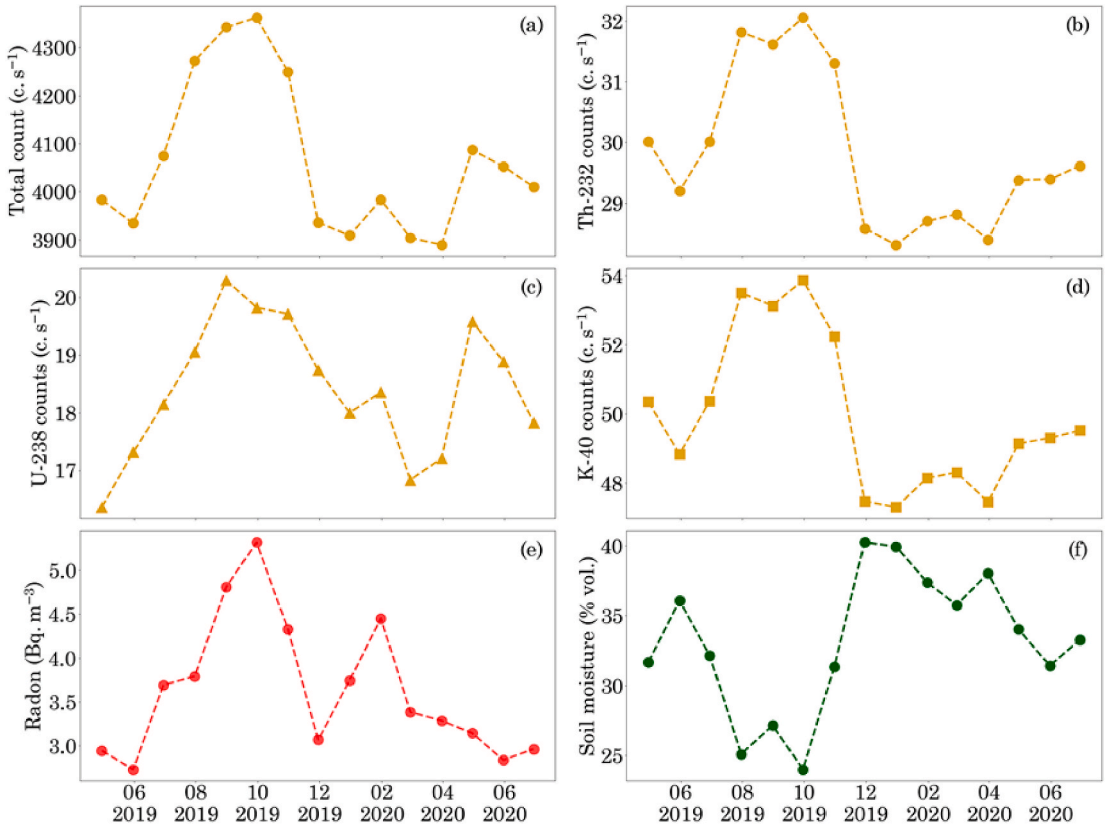

Fig. 6. The pattern of monthly average (a) total count in c s^{-1}, (b) Th-232 counts in c s^{-1}, (c) U-238 counts in c s^{-1}, (d) K-40 counts in c s^{-1}, (e) Atmospheric radon concentration in Bq m^{-3} and (f) Soil moisture content (% vol.), over the period April 2019–June 2020. Significantly different patterns occur at summer and winter time illustrating the correlation or anticorrelation between gamma-ray signal and environmental factors. Rainfall events are excluded from the dataset.

increasing the count rate in the U window due to ^{214}Bi produced by atmospheric radon-222.

The observed correlations and anticorrelations between the different temporal series therefore reflect a strong influence of the environmental factors on the time evolution of the gamma-ray signal.

3.2. Effect of environmental factors on the airborne gamma-ray signal

3.2.1. Atmospheric pressure

Cosmic ray-induced radiations constitute one of the sources of background. This cosmic background is due to the interaction between secondary radiations, produced by the interaction of primary charged particles of cosmic or solar origin with the atmosphere, with the NaI(Tl) detector. Since gamma-rays emitted by radionuclides from the ^{238}U, ^{232} Th day series and by ^{40}K have energies below that of ^{208}Tl at 2615 keV (except a few gamma rays from ^{214}Bi with extremely low yields), all the counts measured in the 2900–3066 keV energy range window of the NaI(Tl) spectrometer result from such interactions. The 2900–3066 keV energy range is therefore referred to as the cosmic counts window.

There are several variables that could affect the intensity of this signal, such as solar activity, atmospheric pressure, location and altitude of the detector.

Over this 14 month-campaign, we investigated how atmospheric pressure affects the number of secondary cosmic radiations detected. The result is presented in Fig. 7. A strong negative linear correlation between the cosmic count rate in c s^{-1} and atmospheric pressure was found with a Pearson correlation coefficient of 0.76. This negative correlation is called the barometric effect (Myssowsky and Tuwim, 1926; de Vries, 2012).

An increase in air pressure of 50 mbars leads to a decrease of approximately 0.4 c s^{-1} in the cosmic counts window. Over this energy range, each crystal of the detector measured approximatively the same cosmic counts with a mean value of 0.45 c s^{-1}.

Strickly speaking, the atmospheric pressure therefore influences the correction to be applied to the count rates. Here, we applied a mean cosmic correction derived from the whole dataset of 2.85, 2.48 and 1.87 c s^{-1} for the energy windows of ^{40}K, ^{238}U, ^{232}Th, respectively. These values were obtained by extrapolating the mean spectrum obtained in the 2900–3066 keV energy range (with 30 keV bins) to lower energies, using a power law.

A Fourier analysis was performed on the whole dataset, rainfall events included, for the ^{232}Th, ^{40}K and cosmic count rates, for atmospheric pressure, temperature and for soil humidity (Fig. 8a). In addition to a diurnal cycle that will be discussed in association with soil humidity variations (see Section 3.2.3), the Fourier spectra of ^{232}Th and ^{40}K count rates reveal the presence of a semi-diurnal cycle that is also clearly visible in the pressure and temperature spectra (Fig. 8a) and in the daily average of atmospheric pressure derived from the whole dataset (Fig. 8b). This correlation could have two explanations, which could act in concert. Indeed, variations of atmospheric pressure will induce variations of gamma-ray attenuation (with higher pressures leading to lower signals), but also variations in cosmic ray background (with higher pressures leading to lower cosmic background, and thus to lower signal as well). However, the Fourier spectrum of the cosmic count rate does not reveal any detectable diurnal nor semi-diurnal variations, which suggests that the effect of pressure on gamma-ray attenuation is dominant in the 12 h signal. The pressure and temperature spectra also exhibit characteristic frequencies with periods of 8 and 6 h, which seem to be too faint to induce detectable variations in the gamma-ray signal. The periods of 24, 12, 8 and 6 h seen in these spectra result from thermal atmospheric tides, which are known to be rich in harmonics.

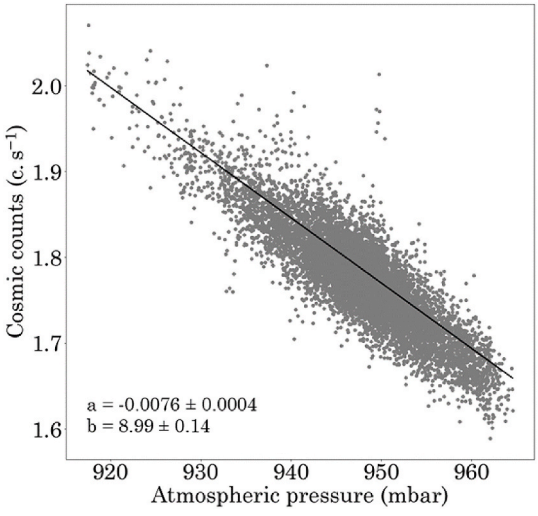

Fig. 7. Cosmic counts in c s^{-1} in the energy window 2900–3066 keV as a function of the atmospheric pressure in mbar. A strong negative correlation is observed with a $R^2 = 0.76$. The linear fit is represented by the black line.

3.2.2. Rainfall events

We identified 2517 hourly data points associated with a rainfall event, as measured by the rain gauge, representing a total of 24.8% of the data. We observed different patterns of precipitations over the year like short intense rains lasting a few minutes or a succession of light drizzle for several hours. Precipitations can have a large effect on the count rates in the U window and thus on the total count rate as well, as seen in the time series of the gamma-ray total counts, U count rate and rainfall intensity shown in Fig. 9. Rainfall events are associated with spikes in the total count rate and in the U count rate.

Fig. 10 (a) shows a positive relationship between the rainfall intensity in mm h^{-1} and the increase in the uranium count rate window in percent. This trend is established from the analysis of 278 individual rain episodes. It reflects the increase of the efficiency of the washout of radon-222 progeny (^{214}Pb and ^{214}Bi), which behave as free aerosols or attach themselves to other aerosols in the atmosphere with rainfall intensity, which appears to be linear over this range of rainfall intensities ($R^2 = 0.95$).

Over the whole dataset, we observe a typical rainfall effect on the count rate in the U window, which could lead to an overestimation of U concentration in the ground by a factor ranging from 10 to 300%, with an average value of 30% (over a terrain containing an average uranium abundance of 38.9 Bq kg^{-1}). Charbonneau and Darnley (1970) observed an even stronger effect, with an overestimation of more than 2000% of the concentration of U in the ground.

Each individual rainfall episode has typically an influence on the gamma spectra for ~3 h (after the end of the rainfall event), corresponding to the time necessary for the deposited short-lived radon-222 progenies to decay. The disturbed signal then reaches a level below the one measured prior to the rainfall event due to a persistent increase of soil moisture associated with the precipitations (yellow dashed line in Fig. 10 (b)).

3.2.3. Soil moisture

Soil moisture has a strong effect and varies on different timescales, due to the gradual drying of soils and to precipitation events.

The Fourier spectra of ^{232}Th and ^{40}K count rates reveal the presence of a strong diurnal cycle (period of 24 h), which is also seen in the soil humidity spectrum (Fig. 8a). Both are probably related to the diurnal variations of surface temperature. Larger temperatures reduce soil moisture, which in turn increase the gamma-ray signal, as seen in figure (Fig. 11), which represents the global average daily cycles of ^{232}Th count rate and soil moisture (0–5 cm). The small time lag between the two curves can be explained by the inertia of the soil drying/humidification process over this depth range, while the increase of the gamma-ray signal starts as soon as the surficial layer is drying up or wetting. The

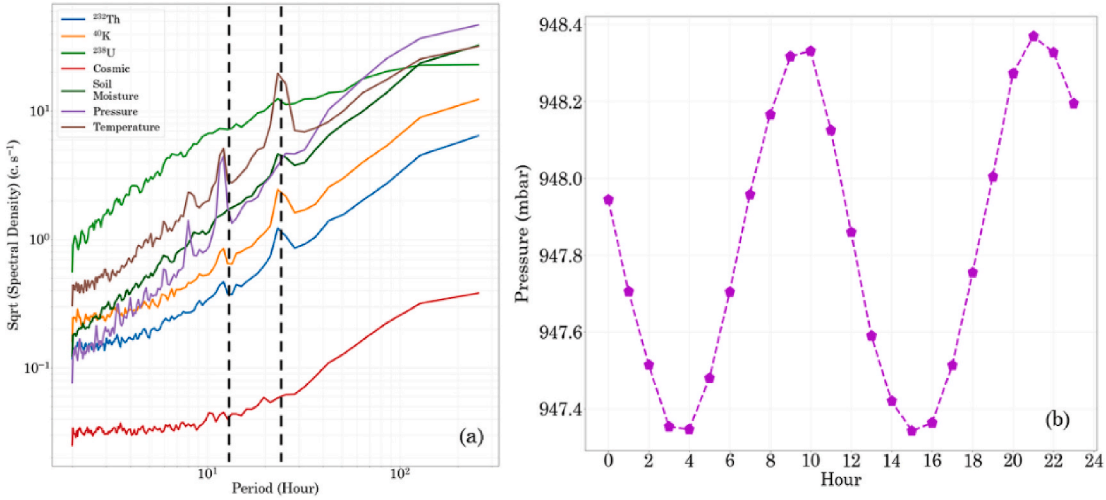

Fig. 8. (a) Fourier analysis of the ^{232}Th, ^{238}U and ^{40}K count rates and on soil moisture and atmospheric pressure for the whole dataset. A 12 and 24-h cycle is observed for both ^{232}Th and ^{40}K but not as clearly for ^{238}U (except a small peak at 24 h). (b) Atmospheric pressure vs hour of the day for the whole dataset. A 12 and 24-h cycle is also observed for atmospheric pressure.

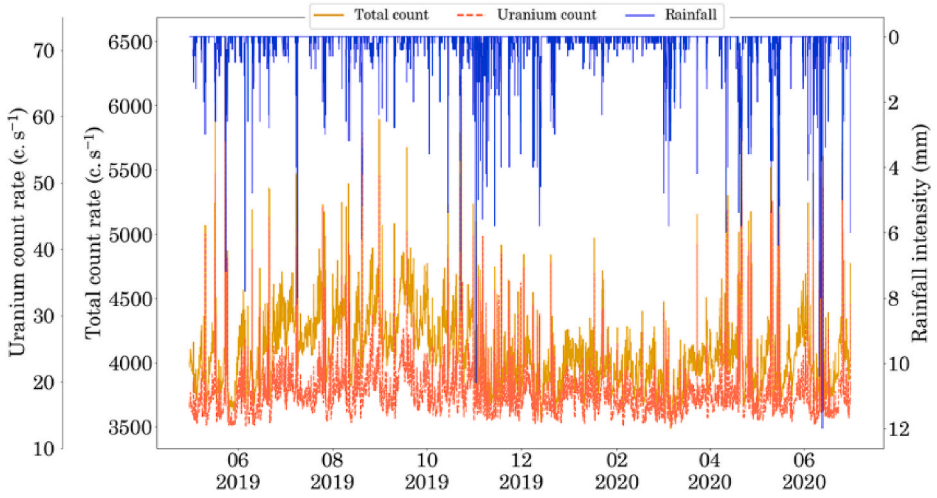

Fig. 9. Time series of total count rate in c s^{-1}, U count rate in c s^{-1} and rainfall intensity in mm h^{-1} as recorded at the Centre de Recherches Atmosphériques (P2OA-CRA) in Lannemezan between April 2019 and June 2020.

small early morning increase in the ^{232}Th count rate (~3–4 a.m.) is related to the semi-diurnal variation of atmospheric pressure reaching a minimum over this time period, as discussed in section 3.2.1 (Fig. 8b). The same effects are observed with the ^{40}K count rate (not shown).

The observed relationship between the airborne ^{232}Th, ^{40}K and ^{238}U count rates, and the degree of water saturation in the soil is shown in Fig. 12. A variation of 24% of the volumetric soil moisture between dry (19%) and wet conditions (43%) induces a reduction by 23.6% of the ^{232}Th count rate from 34 to 27.5 c s^{-1} (Fig. 12a) and by 23.9% of the ^{40}K count rate from 57 to 46 c s^{-1} in Fig. 12b. Accordingly, two airborne surveys performed in summer and in winter could show notable differences, up to 25% for the radionuclides concentration measured at P2OA-CRA, which is not due to the migration of radionuclides in the soil but generated by variations of soil moisture.

A linear relationship exists between the attenuation coefficient and the soil moisture content (*e.g.* Grasty and Minty, 1995; Cook et al., 1996; Minty et al., 1997; IAEA, 2003). The gamma-ray signal measured by a spherical detector at an elevation h above the ground varies with soil moisture content with parameters and notations adapted from Kogan et al. (1971) and Grasty (1975) as:

$$\Phi(w) = \frac{A\,\eta\,n\,E_2(\mu h)}{2\left[\widehat{\mu}_s\,\rho_s\varepsilon_0 + \widehat{\mu}_w\,\rho_w\,\varepsilon_0 S_w\right]} = \frac{A\,\eta\,n\,E_2(\mu h)/2}{\widehat{\mu}_s\,\rho_{b,\,dry} + \widehat{\mu}_w\,\rho_w\,w} = \frac{a}{b + c\,w} \tag{1}$$

where $\Phi(w)$ is the gamma-ray count rate, A is the cross-sectional area of the detector, η is the photopeak detection efficiency, n the number of photons emitted by unit volume of soil, E_2 is the exponential integral of the second kind, h is the height of the detector above ground, μ is the linear attenuation coefficient in air, and are the gamma-ray attenuation coefficients by unit mass of solid matter and water, respectively, ρ_s is the solid density of the soil constituent, $\rho_{b,dry}$ is the dry bulk density of the soil, ρ_w is the water density, S_w and w are the volumetric soil moisture contents by unit volume of pore space and soil, respectively, and is the dry porosity.

By using Equation (1), we can fit the measured count rates as a function of soil moisture. The water density was set to a fixed value of 1000 kg m^{-3} and the attenuation coefficients in the soil and in water are those from NIST for each radionuclide (Table 3). These parameters, and thus the parameter c of Equation (1), are fixed in the fitting procedure.

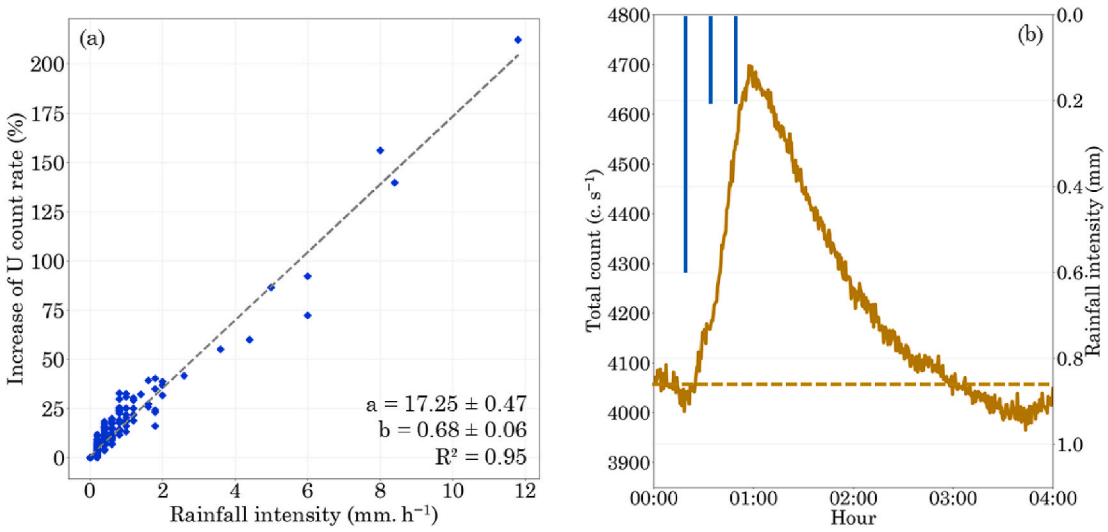

Fig. 10. (a) Increase of the uranium count rate (in %, hourly averages) due to individual precipitation events as a function of rainfall intensity in mm h-1 ($R^2 = 0.95$). (b) Individual precipitation event with a rapid increase of the gamma-ray total count followed by a ~3 h-long decay of short-lived radon decay products. The dashed line represents the mean value before the rainfall event.

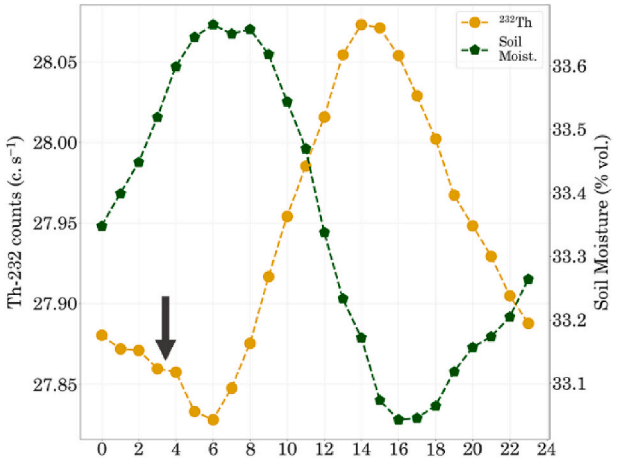

Fig. 11. Global average daily cycle of ^{232}Th count rate (c s^{-1}) and soil moisture (0–5 cm depth). The small increase of ^{232}Th count rate indicated by the arrow corresponds to the minimum atmospheric pressure shown in Fig. 8b.

The parameters *a* and *b* are adjusted by a least-square method. The dry bulk soil density is then derived from the parameter *b*.

As seen in Fig. 12, there is a good agreement between the theoretical fit based on Equation (1) and the data, rainfall events excluded. The value of the dry bulk density obtained from each theoretical fit (1185 kg m^{-3} for ^{232}Th, 1210 kg m^{-3} for ^{40}K and 1160 kg m^{-3} for ^{238}U), is very similar to the dry bulk density measured *in situ* (1200 ± 44 kg m^{-3}).

The inverse proportionality observed between the gamma-ray count rate and the soil bulk density, which has a linear dependence with soil moisture, describes the measured variations of ^{232}Th and ^{40}K very well, and agrees with previous studies (Carroll, 1981; Grasty, 1997; Baldoncini et al., 2019). Equation (1) is not sufficient, however, to account for the variability observed for ^{238}U, which shows deviations of up to 50% from the theoretical fit (Fig. 12c).

Soil moisture could therefore be the most influential environmental factor on the ^{232}Th and ^{40}K count rates, but it cannot explain by itself the dispersion shown in the uranium count rate.

3.2.4. Atmospheric radon

The presence of radon-222 in the atmosphere constitutes another important source of background. With its relative long half-life, this gas is frequently used for atmospheric studies (Jacobi and André, 1963; Genthon and Armengaud, 1995; Jacob et al., 1997; Zahorowski et al., 2004; Meslin et al., 2006; Williams et al., 2011; Florea and Duliu, 2012; Botha et al., 2018). While ^{40}K and ^{232}Th (^{208}Tl) are mostly distributed in the soil, ^{214}Bi-gamma radiation, used to measure ^{238}U, has an atmospheric component due to the exhalation of radon-222 produced in the soil. The radon-222 activity level measured at one location can have a local or regional origin and can vary with several environmental factors such as wind speed and wind direction.

Its exhalation rate varies mainly with U concentration in the soil, soil moisture, porosity and to a lower extent, permeability (Ball et al., 1991; Meslin et al., 2011; Griffiths et al., 2010; Karstens et al., 2015). The average radon-222 exhalation rate for the Earth's surface is 20 mBq m^{-2} s^{-1} (Whittlestone et al., 2006).

As seen in Figs. 5d and 6e, the observed radon-222 vol activity ranges from 0.5 to 14 Bq m^{-3} with the highest monthly mean value occurring in the beginning of fall when the soil is driest. In addition, a difference in radon concentration was observed between the three heights (1 m, 30 m and 60 m) during most of the nights, indicating the presence of a negative vertical gradient at night. The seasonal variations of radon concentration, however, were similar at all heights. As a rule, the atmospheric radon-222 concentration was found to be larger during nighttime than during daytime, due to the stable thermal stratification and low turbulent mixing of air at night.

In order to observe the influence of atmospheric radon-222 on the ^{214}Bi measurement in the time series, we investigated the variations of uranium count rate, radon-222 concentration and soil moisture over the 00 h–06 h time span. Indeed, if an increase of U count rate and radon-222 activity concentration is observed during this time period while the soil moisture remains constant (because it is colder than in the day), then this increase can be attributed to atmospheric radon-222.

An example of a typical nighttime radon-222 event, observed on May 2nd, 2019 is presented in Fig. 13, which compares the 1 h-averaged ^{238}U (^{214}Bi) count rate in c s^{-1} (Fig. 13a), the soil moisture content in volume percentage (Fig. 13b) and the atmospheric radon-222 activity in Bq m^{-3} (Fig. 13c). The soil moisture content is constant over the 6 h-timeframe with an average value of 29.5% vol. and a dispersion of 0.01% vol. during this event. The patterns of uranium count rate and atmospheric radon-222 are very similar with a peak maximum observed at 1 a.m.

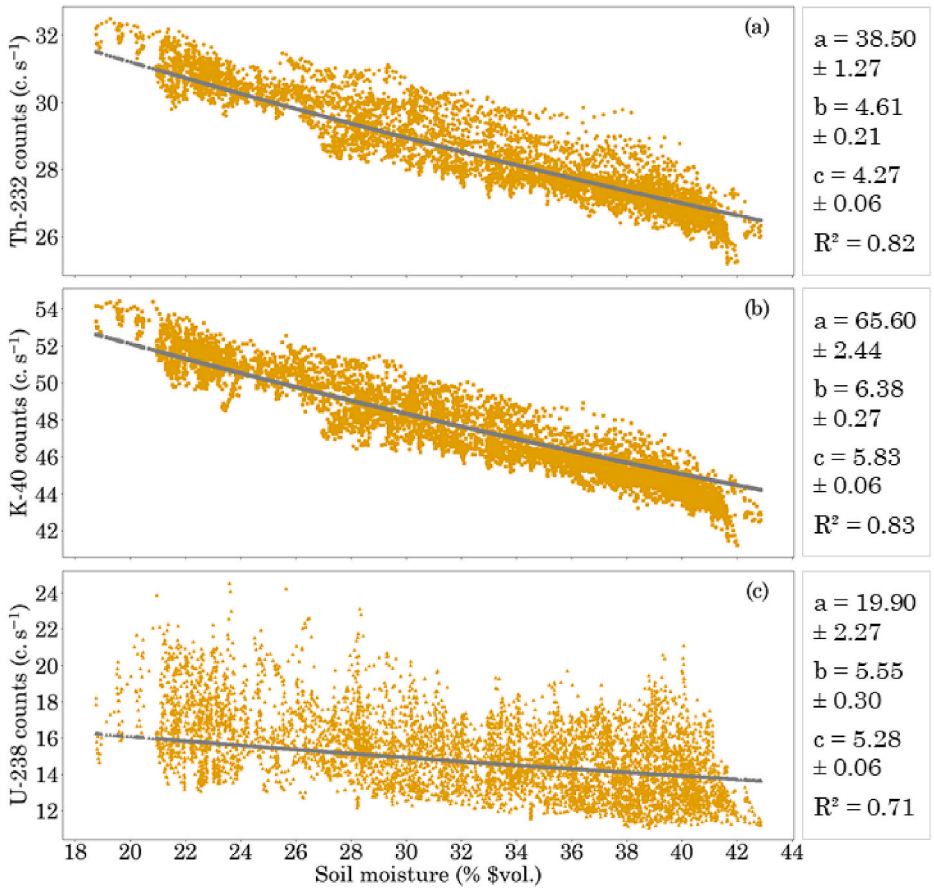

Fig. 12. Gamma count rates in c s^{-1} for ^{232}Th (a), ^{40}K (b) and ^{238}U (c) as a function of soil moisture content (using hourly averages). The gray line represents the curve fit from equation (1). The parameters and the determination coefficient for each theoretical fit are presented. The rainfall data are excluded from this analysis.

Table 3
Attenuation coefficients in the soil (supposed to be SiO_2) and in water.

Element	Isotope	(m^2 kg^{-1})	(m^2 kg^{-1})
Potassium	^{40}K	5.26×10^{-3}	5.83×10^{-3}
Uranium	^{214}Bi	4.77×10^{-3}	5.29×10^{-3}
Thorium	^{208}Tl	3.89×10^{-3}	4.27×10^{-3}

(16.8 c s^{-1}, 4.7 Bq m^{-3}) followed by a constant decrease until 6 a.m. A loss of 1.36 c s^{-1} is associated with an atmospheric radon-222 decrease of 2 Bq m^{-3}. A 40% increase of atmospheric radon-222 activity concentration (1.33 Bq m^{-3}) leads to a 5% increase in the uranium count rate (0.75 c s^{-1}) between 1 a.m. and 2 a.m.

We have identified at least 350 clear radon-222 events in the whole dataset with a mean increase of 1.30 ± 0.08 c s^{-1} for an atmospheric radon-222 activity concentration of 2.00 ± 0.21 Bq m^{-3}. The atmospheric radon-222 activity influences the uranium count rate by ± 3.8%/Bq m^{-3}. This value is obtained for a mean soil ^{238}U concentration of 38.9 Bq kg^{-1} dry soil. Since the contributions from the subsurface and atmospheric components to the U signal are independent of each other and are summed-up, this influence can be scaled by the uranium concentration in the soil measured at P2OA-CRA, so that it can be extrapolated to any other site whose uranium concentration is known. This yields an influence of 148%/Bq m^{-3} for a soil containing 1 Bq kg^{-1} of uranium, or 148%/Bq m^{-3}/kg Bq^{-1}(U), as the relative contribution of the atmospheric compartment decreases as the U concentration in the soil increases.

Fig. 14 shows the difference between the apparent ^{238}U count rate and the theoretical fit of Fig. 12 as a function of radon-222 activity in Bq m^{-3}. A 3-h running mean was applied to the dataset. A strong linear relationship between those parameters was found. Radon-222 seems to be responsible for the largest difference observed between the ^{238}U count rate and the theoretical fit.

Radon-222 variations and rainfall events probably obscure the 12 h and 24 h frequencies for uranium in the Fourier analysis shown in Fig. 8a, although a small peak at 24 h is observed. The near-surface accumulation of radon at night (which increases the apparent uranium) is indeed out of phase with respect to the daily minimum moisture responsible for the increase of the gamma-ray signal discussed earlier. The impact of radon-222 on an airborne gamma-ray survey is therefore far from negligible and will of course vary with the atmospheric radon-222 activity at the time of the survey. For example, at P2OA-CRA, this impact could vary by a factor of 28 between the two extremes of the time series for a day in winter and a day in summer.

4. Conclusions

Over a 14 month continuous campaign from April 2019 to June 2020 we simulated a hover flight or airborne gamma-ray survey at a typical altitude of 50 m with a NaI(Tl) spectrometer, at the Pyrenean Platform for Observation of the Atmosphere (P2OA) on the Centre de Recherches Atmosphériques site, in Lannemezan, France.

The influence of key environmental parameters such as atmospheric pressure, rainfall, soil moisture and atmospheric radon-222 on the gamma-ray signal was investigated. Each of these parameters can have a significant influence:

- The negative linear correlation between air pressure and cosmic count rate is observed with this long-term monitoring. Variations in atmospheric pressure lead to fluctuations of the cosmic count rate

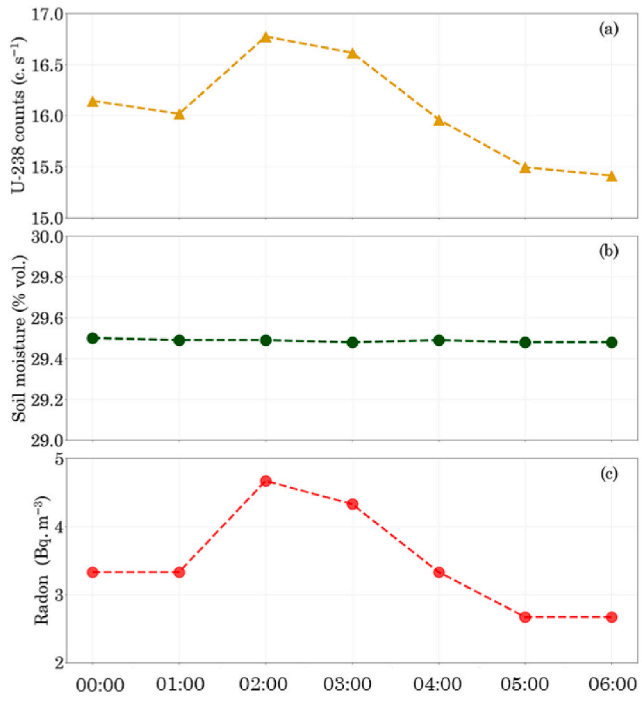

Fig. 13. (a) U count rate in c s^{-1} as a function of time, (b) Soil moisture content in % vol. as a function of time and (c) atmospheric Rn concentration in Bq m^{-3} as a function of time for an identified radon-222 event occurring overnight on the 2nd May 2019. The patterns of U count rate and Rn concentration are very close, whereas the soil moisture content remains almost constant during the event.

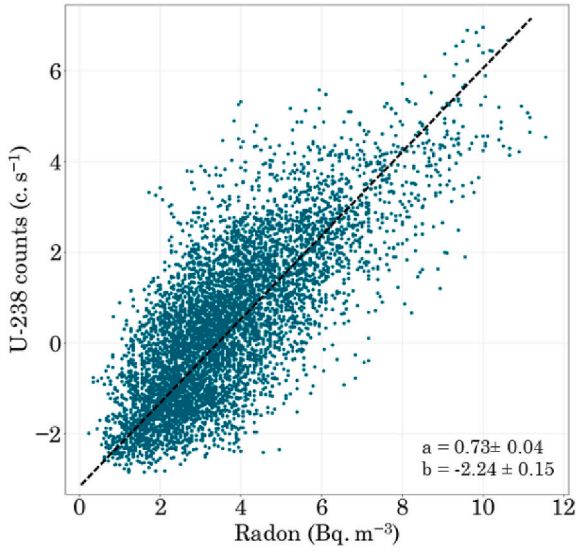

Fig. 14. Difference between the effective ^{238}U count rate and the theoretical fit (c s^{-1}) shown in Fig. 8 (c) as a function of radon concentration (Bq m^{-3}) measured by the AlphaGuards. A 3-h running mean was performed on the data to attenuate the statistical fluctuation. The negative values along the y-axis at low radon concentrations result from the fact that the fit shown in Fig. 12 (c) is applied to the raw data, i. e, not corrected for the effect of atmospheric radon. As a result, large radon concentrations tend to push the fit upward.

used in the data processing of approximately 5% for 10 mbar. The semi-diurnal variation of atmospheric pressure, related to thermal atmospheric tides, also induces a semi-diurnal variation of the apparent ^{232}Th and ^{40}K concentrations, which results from a weaker gamma-ray attenuation when the pressure decreases, rather than an increase of the cosmic background.

- Rainfall events can increase the uranium count rate by 300% and the total count rate by 100%. A 3-h period is needed to completely remove the anomalous count rate stemming from the washout of radon-222 progeny.
- Soil moisture has an average value of 25%, varying from 18% in summer to 43% in winter. The same amount of variation is observed for the thorium and potassium count rates but not for the uranium count rate. The diurnal cycle of soil moisture also induces a diurnal cycle in apparent ^{232}Th and ^{40}K concentrations.
- The atmospheric radon-222 activity influences the uranium count rate by about ±3.8% per Bq m^{-3} for a soil ^{238}U concentration of 38.9 Bq kg^{-1} dry soil, which translates into an influence of 148%/Bq m^{-3}/kg Bq $^{-1}$(U) for other sites.

The observed temporal variations of the total count rate were related to the evolution of one of the above environmental factors. The effect of potassic and phosphate fertilizers inputs was not assessed in this study due to the absence of such agricultural practices in the field of view of the spectrometer.

Precise measurements of K, U, Th and artificial radionuclides, for example to study their mobility in the environment over long time periods, or to monitor their spatial distribution for geological or radiological surveys, depend crucially on the knowledge of these factors. Future work will focus on the implementation of corrections needed to account for the variations of such factors. This study also follows-up with the work of Baldoncini et al. (2019) in showing the potential of gamma-ray spectrometry for long-term monitoring of soil moisture at a scale (~200 m in this study) intermediate between *in situ* and satellite observations.

Declaration of competing interest

The authors declare that they have no known competing financial interests or personal relationships that could have appeared to influence the work reported in this paper.

Acknowledgements

This study was funded by the French Atomic Energy Commission (CEA) assisted by the Université Paul Sabatier, Toulouse, as a part of a PhD thesis. We gratefully acknowledge CEA for providing the NaI(Tl) spectrometer, the radon-222 monitors and the soil moisture acquisition system. Observation data were collected at the Pyrenean Platform for Observation of the Atmosphere P2OA (http://p2oa.aero.obsmip.fr). *P2OA facilities and staff are* funded *and* supported *by the University Paul Sabatier, Toulouse, France, and CNRS (Centre National de la Rechercher Scientifique)*. P2OA is a component of the ACTRIS-Fr Research Infra-Structure and benefits from AERIS data centre (https://www.aeris-data.fr/) for hosting service data. The authors would like to thank the Centre de Recherches Atmosphériques (CRA) for their assistance and for the access to meteorological data collected during this field study. The InfoClimat station network was also a contributor of this study. Finally, this paper was improved by the careful work of anonymous reviewers.

References

Baldoncini, M., Albéri, M., Bottardi, C., Chiarelli, E., Raptis, K.G.C., Strati, V., Mantovani, F., 2019. Biomass water content effect on soil moisture assessment via proximal gamma-ray spectroscopy. Geoderma 335, 69–77. https://doi.org/10.1016/j.geoderma.2018.08.012.

Ball, T.K., Cameron, D.G., Colman, T.B., Roberts, P.D., 1991. Behaviour of radon in the geological environment : a review. Q. J. Eng. Geol. Hydrogeol. 24, 169–182.

Beamish, D., 2015. Relationships between gamma-ray attenuation and soils in SW England. Geoderma 259–260, 174–186. https://doi.org/10.1016/j.geoderma.2015.05.018.

Botha, R., Labuschagne, C., Williams, A.G., Bosman, G., Brunke, E.-G., Rossouw, A., Lindsay, R., 2018. Characterising fifteen years of continuous atmospheric radon activity observations at Cape Point (South Africa). Atmos. Environ. 176, 30–39. https://doi.org/10.1016/j.atmosenv.2017.12.010.

Carrier, F., Bourdon, B., Pili, É., Truffert, C., Wyns, R., 2006. Airborne gamma-ray spectrometry to quantify chemical erosion processes. J. Geochem. Explor. 88, 266–270. https://doi.org/10.1016/j.gexplo.2005.08.053. Extended Abstracts presented at the 7th Symp. on the Geochemistry of the Earth's Surface (GES-7).

Carroll, T.R., 1981. Airborne soil moisture measurement using natural terrestrial gamma radiation. Soil Sci. 132, 358–366.

Charbonneau, B.W., Darnley, A.G., 1970. Radioactive Precipitation and its Significance to High Sensitivity Gamma-Ray Spectrometer Surveys. Geological Survey of Canada (Paper 70-1 No. Part B).

Cook, S.E., Corner, R.J., Groves, P.R., Grealish, G.J., 1996. Use of airborne gamma-radiometric data for soil mapping. Aust. J. Soil Res. 34, 183–194. https://doi.org/10.1071/SR9960183.

de Vries, L., 2012. Search for a Correlation between HiSPARC Cosmic-Ray Data and Weather Measurements (Master's Thesis). National institute for subatomic physics, Amsterdam.

Deal, L.J., Doyle, J.F., Burson, Z.G., Boyns, P.K., 1972. Locating the lost Athena missile in Mexico by the aerial radiological measuring system (ARMS). Health Phys. 23, 95–98.

Florea, N., Duliu, O.G., 2012. Eighteen years of continuous observation of Radon and Thoron progenies atmospheric activity. J. Environ. Radioact. 104, 14–23. https://doi.org/10.1016/j.jenvrad.2011.10.002.

Genthon, C., Armengaud, A., 1995. Radon 222 as a comparative tracer of transport and mixing in two general circulation models of the atmosphere. J. Geophys. Res. Atmospheres 100, 2849–2866. https://doi.org/10.1029/94JD02846.

Grasty, R.L., 1997. Radon emanation and soil moisture effects on airborne gamma-ray measurements. Geophysics 62, 1379–1385. https://doi.org/10.1190/1.1444242.

Grasty, R.L., 1975. Uranium measurement by airborne gamma-ray spectrometry. Geophysics 40, 503–519.

Grasty, R.L., Hovgaard, J., Multala, J., 1997. Airborne gamma-ray measurements in the Chernobyl plume. Radiat. Protect. Dosim. 73, 225–230. https://doi.org/10.1093/oxfordjournals.rpd.a032139.

Grasty, R.L., Minty, B.R.S., 1995. A guide to the technical specifications for airborne gamma-ray surveys. AGSO Aust. Geol. Surv. Organ. Rec. 199660. ISSN: 1039-0073. ISBN: 0 642 22366 1.

Griffiths, A.D., Zahorowski, W., Element, A., Werczynski, S., 2010. A map of radon flux at the Australian land surface. Atmos. Chem. Phys. 10, 8969–8982. https://doi.org/10.5194/acp-10-8969-2010.

IAEA, 2003. Guidelines for Radiolement Mapping Using Gamma Ray Spectrometry (Technical Report No. Report Series, No. 136). International Atomic Energy Agency, Vienna.

IAEA, 1991. Airborne Gamma-Ray Spectrometer Surveying. Technical report No. 323. Vienna.

Jacob, D.J., Prather, M.J., Rasch, P.J., Shia, R.-L., Balkanski, Y.J., Beagley, S.R., Bergmann, D.J., Blackshear, W.T., Brown, M., Chiba, M., Chipperfield, M.P., Grandpré, J. de, Dignon, J.E., Feichter, J., Genthon, C., Grose, W.L., Kasibhatla, P.S., Köhler, I., Kritz, M.A., Law, K., Penner, J.E., Ramonet, M., Reeves, C.E., Rotman, D. A., Stockwell, D.Z., Velthoven, P.F.J.V., Verver, G., Wild, O., Yang, H., Zimmermann, P., 1997. Evaluation and intercomparison of global atmospheric transport models using 222Rn and other short-lived tracers. J. Geophys. Res. Atmospheres 102, 5953–5970. https://doi.org/10.1029/96JD02955.

Jacobi, W., André, K., 1963. The vertical distribution of radon 222, radon 220 and their decay products in the atmosphere. J. Geophys. Res. 68, 3799–3814. https://doi.org/10.1029/JZ068i013p03799, 1896-1977.

Karstens, U., Schwingshackl, C., Schmithüsen, D., Levin, I., 2015. A process-based 222Rn flux map for Europe and its comparison to long-term observations. Atmos. Chem. Phys. 15, 17397–17448. https://doi.org/10.5194/acpd-15-17397-2015.

Kogan, R.M., Nazarov, I.M., Fridman, ShD., 1971. Gamma spectrometry of natural environments and formations-Theory of the method, applications to geology and geophysics. Isr. Program Sci. Trans 5778.

Løvborg, L., 1984. The Calibration of Portable and Airborne Gamma-ray Spectrometers: theory, Problems, and Facilities. Risø-M. Risø National Library. Risø National Library, Roskilde.

Meslin, P.Y., Sabroux, J.C., Bassot, S., Chassefière, E., 2011. Experimental study of radon production and transport in an analogue for the Martian regolith. Geochem. Cosmochim. Acta 75, 2256–2270. https://doi.org/10.1016/j.gca.2011.01.028.

Meslin, P.-Y., Sabroux, J.-C., Berger, L., Pineau, J.-F., Chassefière, E., 2006. Evidence of 210Po on martian dust at meridiani planum. J. Geophys. Res. Planets 111. https://doi.org/10.1029/2006JE002692.

Minty, B.R.S., 1997. Fundamentals of airborne gamma-ray spectrometry. AGSO J. Aust. Geol. Geophys. 17, 39–50.

Minty, B.R.S., Luyendyk, A.P.J., Brodie, R.C., 1997. Calibration and data processing for airborne gamma-ray spectrometry. AGSO J. Aust. Geol. Geophys. 17, 51–62.

Myssowsky, L., Tuwim, L., 1926. Unregelmäßige intensitätsschwankungen der höhenstrahlung in geringer seehöhe. Z. Phys. 39, 146–150.

Punniyakotti, J., Lakshmi, K.S., Meenakshisundaram, V., Manju, N., Poonguzhali, P., 2020. Influence of fertilizers on the natural radioactivity profile of soil samples of agricultural land in Villupuram District, Tamilnadu State, India. J. Radioanal. Nucl. Chem. 325, 85–92. https://doi.org/10.1007/s10967-020-07210-9.

Sanada, Y., Torii, T., 2015. Aerial radiation monitoring around the Fukushima Dai-ichi nuclear power plant using an unmanned helicopter. J. Environ. Radioact. 139, 294–299. https://doi.org/10.1016/j.jenvrad.2014.06.027.

Tourlière, B., Perrin, J., Le Berre, P., Pasquet, J.F., 2003. Use of airborne gamma-ray spectrometry for kaolin exploration. J. Appl. Geophys. 53, 91–102. https://doi.org/10.1016/S0926-9851(03)00040-5.

UNSCEAR, 2000a. Report of the United Nations Scientific Committee on the Effects of Atomic Radiation to the General Assembly. Annex B : Exposures from Natural Radiation Sources.

UNSCEAR, 2000b. Report of the United Nations Scientific Committee on the Effects of Atomic Radiation to the General Assembly. Annex C : Exposures to the Public from Man-Made Sources of Radiation.

Whittlestone, S., Zahorowski, W., Schery, S., 2006. Radon flux variability with season and location in Tasmania, Australia. J. Radioanal. Nucl. Chem. 236, 213–217. https://doi.org/10.1007/bf02386345.

Wilford, J., 2012. A weathering intensity index for the Australian continent using airborne gamma-ray spectrometry and digital terrain analysis. Geoderma 183–184, 124–142. https://doi.org/10.1016/j.geoderma.2010.12.022.

Wilford, J.R., Bierwirth, P.N., Craig, M.A., 1997. Application of airborne gamma-ray spectrometry in soil/regolith mapping and applied geomorphology. AGSO J. Aust. Geol. Geophys. 17, 201–216.

Williams, A.G., Zahorowski, W., Chambers, S., Griffiths, A., Hacker, J.M., Element, A., Werczynski, S., 2011. The vertical distribution of radon in clear and cloudy daytime terrestrial boundary layers. J. Atmos. Sci. 68, 155–174. https://doi.org/10.1175/2010JAS3576.1.

Zahorowski, W., Chambers, S.D., Henderson-Sellers, A., 2004. Ground based radon-222 observations and their application to atmospheric studies. J. Environ. Radioact. 76, 3–33. https://doi.org/10.1016/j.jenvrad.2004.03.033. South Pacific Environmental Radioactivity Association: 2002 Conference.